

Entanglement and magnetism in high-spin graphene nanodisks

I. Hagymási

*Department of Physics and Arnold Sommerfeld Center for Theoretical Physics,
Ludwig-Maximilians-Universität München, Theresienstrasse 37, 80333 München, Germany and
Strongly Correlated Systems "Lendület" Research Group, Institute for Solid State Physics and Optics,
MTA Wigner Research Centre for Physics, Budapest H-1525 P.O. Box 49, Hungary*

Ö. Legeza

*Strongly Correlated Systems "Lendület" Research Group, Institute for Solid State Physics and Optics,
MTA Wigner Research Centre for Physics, Budapest H-1525 P.O. Box 49, Hungary*

We investigate the ground-state properties of triangular graphene nanoflakes with zigzag edge configurations. The description of zero-dimensional nanostructures requires accurate many-body techniques since the widely used density-functional theory with local density approximation or Hartree-Fock methods cannot handle the strong quantum fluctuations. Applying the unbiased density-matrix renormalization group algorithm we calculate the magnetization and entanglement patterns with high accuracy for different interaction strengths and compare them to the mean-field results. With the help of quantum information analysis and subsystem density matrices we reveal that the edges are strongly entangled with each other. We also address the effect of electron and hole doping and demonstrate that the magnetic properties of triangular nanoflakes can be controlled by electric field, which reveals features of flat-band ferromagnetism. This may open up new avenues in graphene based spintronics.

PACS numbers: 71.10.Fd, 71.10.Hf, 73.22.-f

I. INTRODUCTION

Up to lately a common stereotype has been that magnetism is primarily attributed to d electron systems. Nowadays more and more supporting evidence emerges that sp electron systems can host also magnetic moments, moreover, the sp magnetism is predicted to be stable even at room temperature¹. After the observation of magnetic moments in defective samples^{2,3}, enormous attention has been paid to monolayer graphene to investigate if it can exhibit long-range magnetic order. The emergence of long-range magnetic order in graphene is expected along the zigzag edges of samples due to their peculiar nature. The existence of such magnetic order has been controversial until the appearance of modern nanofabrication methods due to the poor edge quality in experiments. The recent development of top-bottom techniques allows now us to tailor graphene samples with atomic precision⁴, and the bottom-up synthesis is capable of creating even smaller nanostructures⁵⁻⁷. The most studied nanostructures with zigzag edges are the graphene nanoribbons, hexagonal and triangular nanoflakes. It has been demonstrated that nanoribbons can be accessed by scanning-tunneling lithography⁴ and bottom-up synthesis as well⁸. The theoretically predicted⁹⁻¹⁶ magnetism of nanoribbons with zigzag edges has been corroborated by several indirect experimental evidence^{7,17,18} since direct observation of magnetic moments would require a macroscopic quantity of nanoribbons which is beyond the scope of the present techniques. The fast development of bottom-up techniques triggered the investigation of other geometries, like the hexagonal and triangular nanoflakes. Very recently, a nanoflake close to a triangular shape has been

created with chemical vapour deposition.¹⁹ The hexagonal structure consists of equal number of atoms from both sublattice, while the triangular one is, however, an uncompensated lattice, which has attracted significant attention recently.²⁰⁻²² This interest is due to the topological frustration²¹ caused by the sublattice imbalance which leads to a ground-state degeneracy proportional to the system size.²² The triangular structure is also interesting from another point of view, namely, it has a ground state with nonzero spin, whose magnitude is proportional to the sublattice imbalance according to Lieb's theorem.²³ Thus, unlike in compensated lattices (graphene nanoribbons, hexagonal nanoflakes), where magnetism occurs beyond certain sizes of the zigzag segments, triangular systems are expected to be magnetic for all sizes. The possibility that they can host net magnetic moments has inspired active research in this field. The magnetic properties of these nanodisks have been explored by various techniques, including Hartree-Fock²⁰, density-functional theory (DFT),²⁴ and configuration-interaction methods.^{25,26} In low-dimensional systems correlation effects become important whose proper treatment requires accurate many-body techniques. Besides a few relevant studies for nanoribbons^{15,16,27} and hexagonal structures^{28,29}, such an analysis for triangular structures is still lacking.

Our goal in this paper is to fill this gap by performing large-scale numerical simulations with the unbiased density-matrix renormalization group algorithm (DMRG).³⁰ With the help of the true many-body ground state we can analyze its entanglement structure, furthermore, its total spin can be directly assessed,³¹ which cannot be done in DFT or mean-field calculations. We check

the reliability of mean-field theory for nanodisks by comparing the magnetization to the DMRG results. Furthermore, we compare the ground-state properties away from half-filling with those obtained from configuration interaction methods.

The paper is organized as follows. In Sec. II. we provide the details of our DMRG calculations and describe the main steps of the mean-field approach. In Sec. III. we briefly recall the properties of the noninteracting system and in Sec. III. A our DMRG results are presented using the elements of quantum information theory, while in Sec. III. B the magnetic properties are discussed in the half-filled case and compared to the mean-field results. In Sec. III. C we address the role of hole and electron doping and show that the system displays the features of a flat-band ferromagnetism also away from half band filling.³² Finally, in Sec. IV. we conclude our results.

II. METHODS

We consider the widely used π -band model of graphene to describe the triangular quantum dot including a local Hubbard-interaction term,

$$\mathcal{H} = -t \sum_{\langle ij \rangle} \hat{c}_i^\dagger \hat{c}_j + U \sum_i \hat{n}_{i\uparrow} \hat{n}_{i\downarrow}, \quad (1)$$

where $t = 2.7$ eV is the nearest-neighbor hopping amplitude, and U is the strength of the local Coulomb interaction. In spite of its simplicity, it has been shown that the Hubbard model with properly chosen parameters and fillings can quantitatively reproduce experimental results in graphene systems.^{18,19} However, less attention has been paid to the model's properties on a triangular nanoflake.

To gain some physical insight into the properties of a triangular nanoflake, we apply the mean-field approach first. By neglecting the fluctuation terms in the Hamiltonian (1), we obtain an effective single-particle Hamiltonian

$$\mathcal{H}_{\text{MF}} = -t \sum_{\langle ij \rangle \sigma} \hat{c}_{i\sigma}^\dagger \hat{c}_{j\sigma} + U \sum_{i\sigma} \langle \hat{n}_{i\bar{\sigma}} \rangle \hat{n}_{i\sigma}, \quad (2)$$

where the unknown electron densities, $\langle \hat{n}_{i\bar{\sigma}} \rangle$ are determined by using the standard self-consistent procedure.

To account for the quantum fluctuations and many-body effects, we use the real-space DMRG algorithm^{30,33-37}. We map our short-ranged 2D Hamiltonian to a one-dimensional chain topology with long-range couplings (see Sec. III, Fig. 2). The area law limits the available system sizes since the DMRG cost scales exponentially with the entanglement entropy which is proportional to the size of the triangle. In order to decrease the truncation errors to the order of 10^{-4} , we kept up to 20000 block states. With such a large bond dimension, we were able to determine the many-body ground state and correlation functions accurately.

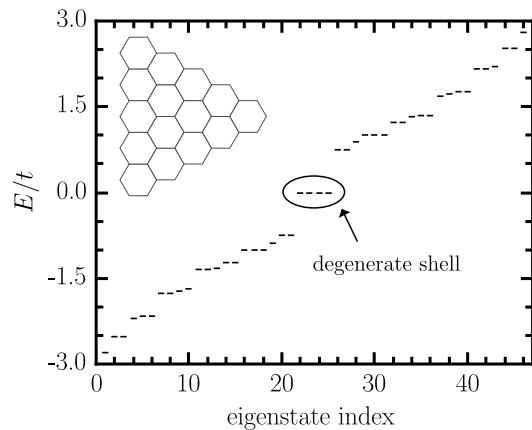


FIG. 1. The energy spectrum of the noninteracting system. The inset shows the investigated system, the circled levels form the degenerate shell at the Fermi level.

III. RESULTS

We start by briefly recalling the properties of the non-interacting case. The system we consider is seen in the inset of Fig. 1. Just like in zigzag nanoribbons zero-energy states appear at the Fermi energy, but here they form a degenerate shell due to the absence of translational symmetry.³⁸ Their degeneracy is $N_{\text{edge}} - 1$ according to the general theorem in triangular nanodisks,²² where N_{edge} is the number of edge atoms along a side of the triangle. These degenerate states are sensitive to electron-electron interaction and play a crucial role – like in the fractional quantum Hall effect³⁹ – and are responsible for the flat-band magnetism³² occurring in the system.

A. Quantum information analysis, correlation functions

First, we examine the ground-state properties of the half-filled system by calculating various correlation functions. We study the correlations between two arbitrary sites within our system, which can be characterized by the mutual information,⁴⁰⁻⁴²

$$I_{ij} = s_i + s_j - s_{ij}. \quad (3)$$

It measures all types of correlations (both of classical and quantum origin) between sites i and j . This quantity is often referred as the strength of entanglement between the two sites embedded in the whole system. Here s_i and s_{ij} are the one- and two-site von Neumann entropies,⁴³⁻⁴⁸ respectively, that can be calculated from the corresponding one- and two-site reduced density matrices,

$$s_i = -\text{Tr} \rho_i \ln \rho_i, \quad (4)$$

$$s_{ij} = -\text{Tr} \rho_{ij} \ln \rho_{ij}, \quad (5)$$

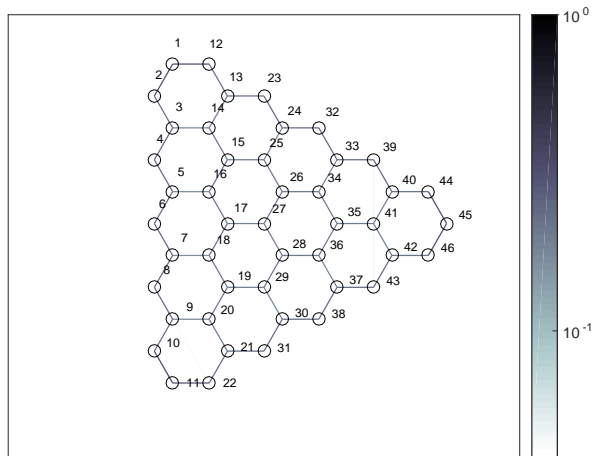


FIG. 2. Entanglement patterns in a zigzag nanodisk for $U = 0$. The magnitude of the mutual information components is encoded using the grayscale in the sidebar. The numbers indicate the positions of sites along the one-dimensional DMRG topology.

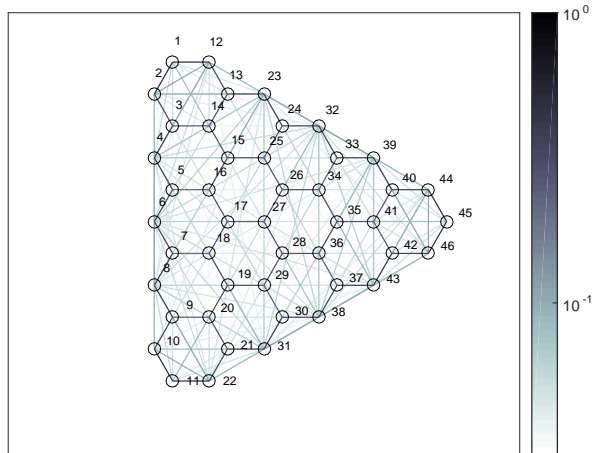


FIG. 3. Similar to Fig. 2 but for $U/t = 2$.

where ρ_i (ρ_{ij}) is the reduced density matrix of site i (sites i and j), which is obtained from the density matrix of the total system by tracing out the configurations of all other sites. In what follows, we explore the entanglement structure of the ground state by calculating the mutual information for different values of the Hubbard interaction to investigate the role of the electron-electron interaction. We begin with the noninteracting case, the entanglement structure within the nanodisk is shown in Fig. 2 for $U = 0$. It is immediately seen that only short-ranged correlation develop between the sites, which is typical for noninteracting systems. This drastically changes as the interaction is switched on, as is seen in Fig. 3 for $U/t = 2$. We can observe that the sites along each zigzag edge becomes correlated, moreover, long-ranged entanglement appears between any two edges. This is somewhat similar to what happens in zigzag nanoribbons, but there are some important differences which will be explained in the

following. The fact that the edge sites are the most entangled can be visualized by considering the correlation values about a given threshold (10^{-2}) and counting the degree of each site. As it can be easily seen from Fig. 4 the edge sites that belong to the zigzag-edge sublattice possess the largest degree.

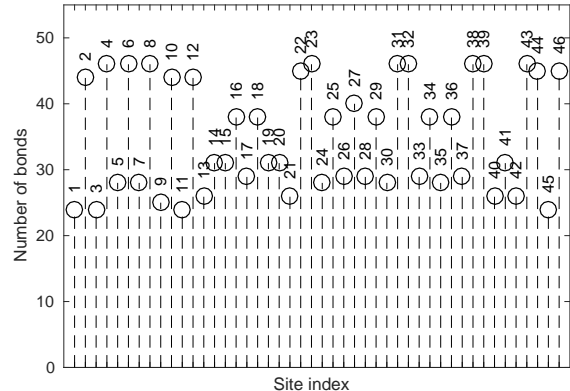


FIG. 4. The degree of lattice sites in Fig. 3 taking into account mutual information bonds larger than 10^{-2} .

The mutual information provides us an overall picture about which sites are strongly correlated with each other. To reveal its origin, it is instructive to investigate the eigensystem of the corresponding two-site density matrices. As a first step, we consider two neighboring zigzag sites at the edge, (4 and 6 in Fig. 3), and solve the eigenvalue problem of the corresponding two-site reduced density matrix, $\rho_{4,6}$. In its eigenvalue spectrum, the most significant eigenvalue ($\omega = 0.13$) is threefold degenerate, and the corresponding eigenvectors are:

$$\begin{aligned}\phi_{4,6}^{(1)} &= |\uparrow\rangle_4 |\uparrow\rangle_6, \\ \phi_{4,6}^{(2)} &= \frac{1}{\sqrt{2}} (|\uparrow\rangle_4 |\downarrow\rangle_6 + |\downarrow\rangle_4 |\uparrow\rangle_6), \\ \phi_{4,6}^{(3)} &= |\downarrow\rangle_4 |\downarrow\rangle_6.\end{aligned}\quad (6)$$

Thus, the electrons in sites 4 and 6 form a triplet. Qualitatively, we have the same result between every pair of sites along a zigzag edge, therefore ferromagnetic correlation emerges at the edges, which is the usual behavior that one expects. It is more interesting to perform this analysis for a pair of sites that are on two adjacent edges, for example 4 and 32. A similar analysis of $\rho_{4,32}$ yields that we have the same eigensystem for the most significant eigenvalue ($\omega = 0.12$) as in the previous case. Based on the strong mutual information between every pair of edges, we can conclude that strong ferromagnetic coupling arises between the edges that has not been reported before. Note that a similar scenario occurs in nanoribbons, namely, the correlations between sites along a zigzag edge are ferromagnetic, too, but there the coupling between the two edges is antiferromagnetic. The

reason is that in the nanoflake the edge sites consist of the same sublattice sites, while in nanoribbons the sites of two zigzag edges belong to the two different sublattices. The nearest-neighbor correlation remains antiferromagnetic in the nanodisk too, which can be seen immediately from the analysis of $\rho_{4,5}$, where the eigenvector belonging to the dominating eigenvalue $\omega = 0.42$ is a singlet:

$$\begin{aligned} \phi_{4,5} = & \\ & 0.59(|\uparrow\rangle_4|\downarrow\rangle_5 - |\downarrow\rangle_4|\uparrow\rangle_5) \\ & + 0.39(|\uparrow\downarrow\rangle_4|0\rangle_5 + |0\rangle_4|\uparrow\downarrow\rangle_5). \end{aligned} \quad (7)$$

The result is qualitatively the same for any nearest-neighbor pair.

B. Magnetic properties at half filling

In the previous subsection the behavior of correlation functions were studied, but – as mentioned in the Introduction – the magnetism of triangular nanodisks is especially interesting since even as small system as ours can exhibit net magnetic moments. We calculate the total spin of the ground state using the spin-spin correlation functions:

$$\langle S^2 \rangle = \left\langle \frac{1}{2} \sum_{ij} (S_i^+ S_j^- + S_i^- S_j^+) + \sum_{ij} S_i^z S_j^z \right\rangle. \quad (8)$$

In the half-filled case we find that the ground state has always $S = 2$ spin for $U > 0$ as it is dictated by the sublattice imbalance ($N_A - N_B = 4$) and Lieb's theorem ($N_A - N_B = 2S$). However, the spin distribution is far from trivial and depends strongly on the Hubbard U . Since the mean-field theory is widely used for the description of graphene nanostructures, we check its predictions for the magnetization.

The results from both methods are shown in Fig. 5 for various values of the Hubbard interaction. In the non-interacting case, the ground state is not unique, therefore we choose the $S_{\text{tot}}^z = 2$ sector to be able to compare the magnetization with the DMRG result. At $U = 0$ both methods give naturally the same result, namely, only the sites of sublattice A (zigzag edge sites, shown by the blue circles) are polarized. Sublattice B can be identified where $\langle S_i^z \rangle = 0$, which was found to be of the order of $10^{-3} - 10^{-4}$ in our DMRG calculations. Switching on U results in the enhancement of nearest-neighbor antiferromagnetic correlations, and as a result, finite magnetization appears on the sites of sublattice B . It is remarkable that the mean-field theory gives quite close results to those of DMRG regarding the magnetization on sublattice A (the difference is around 15%), while it significantly overestimates the polarization on sublattice B , by a factor of 2. The edges carry most of the net magnetic moments. For strong Coulomb interaction, $U/t = 4$, the mean-field theory predicts large polarization inside the nanodisk like along the edges and their values

are grossly overestimated compared to the DMRG results. The failure of the mean-field theory can be traced back to the fact that the infinite honeycomb lattice becomes antiferromagnetic above $U_c/t \sim 2.2$ in the mean-field approach, and our calculation reflects this tendency. The DMRG results also show enhanced magnetization inside the nanoflake, however, their values are still less than the moments appearing at the edges. Larger values of U for graphene are unphysical, since at $U_c/t \sim 3.9$ a Mott transition occurs in the two-dimensional honeycomb lattice.^{49–51}

C. Magnetic properties for electron and hole doping

Lastly, we address the effect of hole and electron doping in the triangular nanoflake. While Lieb's theorem clearly determines the spin of the ground state in the half-filled case, it cannot be used away from half-filling. Previous calculations based on the configuration interaction method pointed out that doping can crucially affect the spin of the ground state.^{25,26} Our findings are summarized in Fig. 6, where the total spin is plotted against the filling of the fourfold degenerate shell in Fig.1.

We find that the maximum spin belongs to the half-filled case, and it gradually decreases as we move away from half filling and it vanishes as soon as the shell is completely filled or becomes empty. What is common with the previous results^{25,26} is that (i) the maximum spin corresponds to the half-filled case, (ii) the nanoflake exhibits magnetization as long as the degenerate shell is partially filled and it disappears if it is fully occupied or no electrons occupy the shell. The configuration interaction method predicts a monotonous decrease of the spin for hole doping, just like in our case, however, for electron doping a non-monotonous behavior is predicted. Namely, when 5 electrons occupy the shell (this means adding a single electron to the half-filled system), a strong depolarization occurs and the ground state has a spin of $S = 1/2$. In contrast, our calculation yields $S = 3/2$ for the same filling. Our results are supported by Mielke's and Tasaki's results for 'flat-band ferromagnetism'.³² In degenerate systems, e.g., in partially filled atomic shells, the ground state has maximal spin (Hund's rule) because a ferromagnetic alignment of the electrons' spins minimizes the Coulomb repulsion at no cost of the kinetic energy. This immediately leads to the pattern seen in Fig. 6. Our results suggest that the triangular nanoflakes may be used as building blocks for spintronic devices, the magnetism is being stable against doping and no complete depolarization occurs which would limit their usability. Since doping can be controlled by an external electric field, it makes the triangular nanoflake an ideal candidate for spintronic applications.

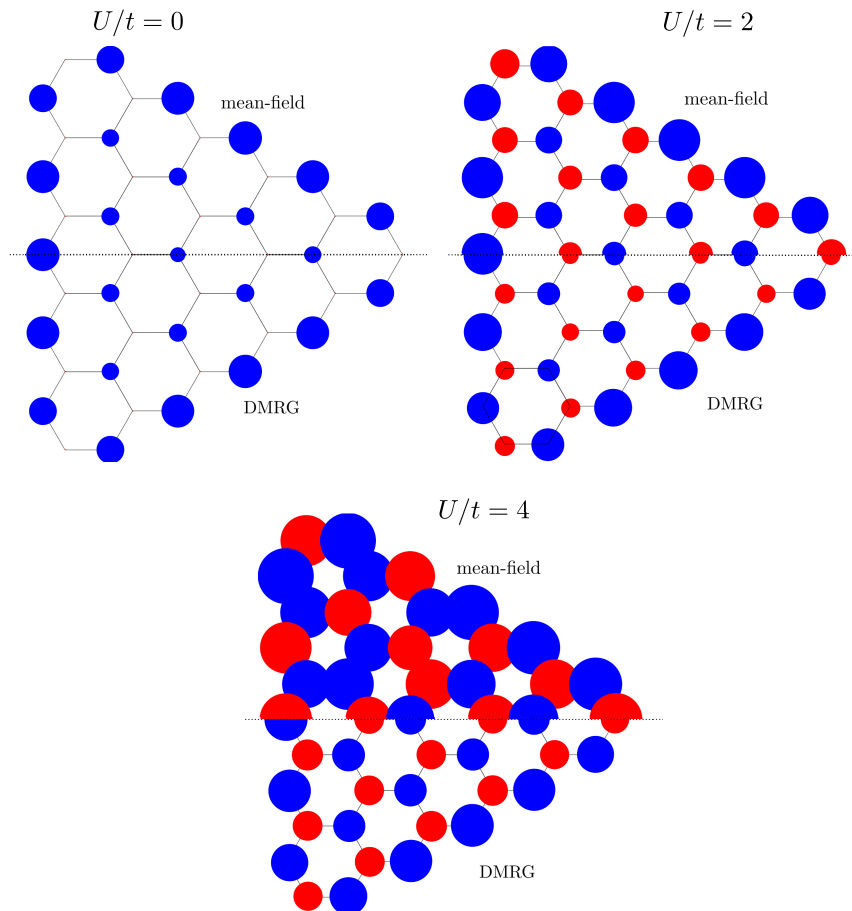


FIG. 5. The local magnetic moments (S_i^z) of the ground for various values of U . The magnitude of up (blue) and down (red) moments are proportional to the area of the circles.

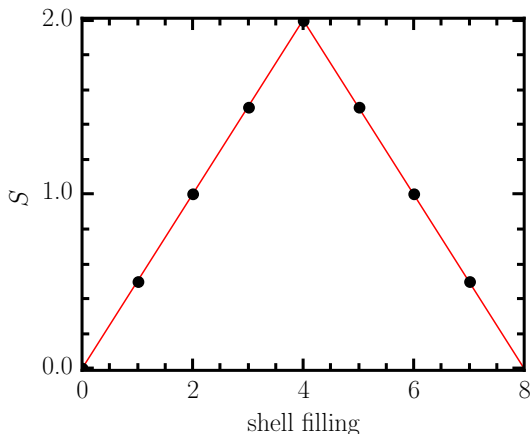


FIG. 6. The ground-state spin for $U/t = 2$ as a function of filling of the fourfold degenerate shell in Fig.1. The line is guide to the eye. The numerical error of S was within the size of the symbols.

IV. CONCLUSIONS

In this paper we examined ground-state properties of triangular graphene nanoflakes by performing large-scale numerical calculations with the unbiased DMRG method. After a short revisit of the noninteracting case, we use the elements of quantum information theory to reveal that strongly entangled edge states emerge in this system. Its source can be attributed to the long-range ferromagnetic correlations between the edges that have not been pointed out so far. We also examined the magnetic properties of the triangular nanodisk and compared the magnetization values to those of mean-field results for various values of the Hubbard interaction. It turned out that for $U/t \sim 2$ the mean-field theory gives fairly good estimates for the edge magnetization, while it overestimates the magnetization in the bulk. Close to the Mott transition, the mean-field approach results in completely wrong magnetization values which is due to the enhanced quantum fluctuations. In each case we obtained a quintet ground state in agreement with Lieb's theorem.

Finally, we considered the effect of electron and hole doping in the system. By calculating the spin correla-

tion functions, the ground-state spin could be unambiguously determined for all possible fillings of the degenerate shell. We found that the ground-state spin decreases gradually as the system is doped away from half-filling and the ground state becomes singlet for a completely empty or full shell, in agreement with the prediction of flat band ferromagnetism. In particular, the high-spin ground state is preserved in the sense that no complete depolarization occurs for small doping.

ACKNOWLEDGMENTS

We acknowledge helpful discussions with F. Gebhard, L. Tapasztó and P. Vancsó. This work was supported in part by the National Research, Development and Innovation Office (NKFIH) through Grant Nos. K120569, NN110360 and within the Quantum Technology National Excellence Program (Project No. 2017-1.2.1-NKP-2017-00001). I.H. is supported by the Alexander von Humboldt Foundation.

-
- ¹ T. Makarova and F. Palacio, eds., *Carbon Based Magnetism* (Elsevier, Amsterdam, 2006).
- ² P. Esquinazi, D. Spemann, R. Höhne, A. Setzer, K.-H. Han, and T. Butz, *Phys. Rev. Lett.* **91**, 227201 (2003).
- ³ R. R. Nair, M. Sepioni, I.-L. Tsai, O. Lehtinen, J. Keinonen, A. V. Krasheninnikov, T. Thomson, A. K. Geim, and I. V. Grigorieva, *Nat. Phys.* **8**, 199 (2012).
- ⁴ L. Tapasztó, G. Dobrik, P. Lambin, and L. P. Biró, *Nat. Nano.* **3**, 397 (2008).
- ⁵ J. Wu, W. Pisula, and K. Müllen, *Chem. Rev.* **107**, 718 (2007).
- ⁶ A. L. Vázquez de Parga, F. Calleja, B. Borca, M. C. G. Passeggi, J. J. Hinarejos, F. Guinea, and R. Miranda, *Phys. Rev. Lett.* **100**, 056807 (2008).
- ⁷ P. Ruffieux, S. Wang, B. Yang, C. Sánchez-Sánchez, J. Liu, T. Dienel, L. Talirz, P. Shinde, C. A. Pignedoli, D. Passerone, T. Dumslaff, X. Feng, K. Müllen, and R. Fasel, *Nature* **531**, 489 (2016).
- ⁸ A. Kimouche, M. M. Ervasti, R. Drost, S. Halonen, A. Harju, P. M. Joensuu, J. Sainio, and P. Liljeroth, *Nat. Commun.* **6**, 10177 (2015).
- ⁹ Y.-W. Son, M. L. Cohen, and S. G. Louie, *Phys. Rev. Lett.* **97**, 216803 (2006).
- ¹⁰ L. Yang, C.-H. Park, Y.-W. Son, M. L. Cohen, and S. G. Louie, *Phys. Rev. Lett.* **99**, 186801 (2007).
- ¹¹ T. Wassmann, A. P. Seitsonen, A. M. Saitta, M. Lazzeri, and F. Mauri, *Phys. Rev. Lett.* **101**, 096402 (2008).
- ¹² J. Fernández-Rossier, *Phys. Rev. B* **77**, 075430 (2008).
- ¹³ O. V. Yazyev, *Phys. Rev. Lett.* **101**, 037203 (2008).
- ¹⁴ J. Jung and A. H. MacDonald, *Phys. Rev. B* **79**, 235433 (2009).
- ¹⁵ H. Feldner, Z. Y. Meng, T. C. Lang, F. F. Assaad, S. Wessel, and A. Honecker, *Phys. Rev. Lett.* **106**, 226401 (2011).
- ¹⁶ I. Hagymási and Ö. Legeza, *Phys. Rev. B* **94**, 165147 (2016).
- ¹⁷ S. Wang, L. Talirz, C. A. Pignedoli, X. Feng, K. Müllen, R. Fasel, and P. Ruffieux, *Nat. Comm.* **7**, 11507 (2016).
- ¹⁸ G. Z. Magda, X. Jin, I. Hagymási, P. Vancsó, Z. Osváth, P. Nemes-Incze, C. Hwang, L. P. Biró, and L. Tapasztó, *Nature* **514**, 608 (2014).
- ¹⁹ I. Hagymási, P. Vancsó, A. Pálinkás, and Z. Osváth, *Phys. Rev. B* **95**, 075123 (2017).
- ²⁰ J. Fernández-Rossier and J. J. Palacios, *Phys. Rev. Lett.* **99**, 177204 (2007).
- ²¹ W. L. Wang, O. V. Yazyev, S. Meng, and E. Kaxiras, *Phys. Rev. Lett.* **102**, 157201 (2009).
- ²² P. Potasz, A. D. Güçlü, and P. Hawrylak, *Phys. Rev. B* **81**, 033403 (2010).
- ²³ E. H. Lieb, *Phys. Rev. Lett.* **62**, 1201 (1989).
- ²⁴ W. L. Wang, S. Meng, and E. Kaxiras, *Nano Letters* **8**, 241 (2008).
- ²⁵ A. D. Güçlü, P. Potasz, O. Voznyy, M. Korkusinski, and P. Hawrylak, *Phys. Rev. Lett.* **103**, 246805 (2009).
- ²⁶ P. Potasz, A. D. Güçlü, A. Wójs, and P. Hawrylak, *Phys. Rev. B* **85**, 075431 (2012).
- ²⁷ M. Golor, S. Wessel, and M. J. Schmidt, *Phys. Rev. Lett.* **112**, 046601 (2014).
- ²⁸ H. Feldner, Z. Y. Meng, A. Honecker, D. Cabra, S. Wessel, and F. F. Assaad, *Phys. Rev. B* **81**, 115416 (2010).
- ²⁹ A. Valli, A. Amaricci, A. Toschi, T. Saha-Dasgupta, K. Held, and M. Capone, *Phys. Rev. B* **94**, 245146 (2016).
- ³⁰ S. R. White, *Phys. Rev. Lett.* **69**, 2863 (1992).
- ³¹ G. Barcza, Ö. Legeza, K. H. Marti, and M. Reiher, *Phys. Rev. A* **83**, 012508 (2011).
- ³² A. Mielke and H. Tasaki, *Comm. Math. Phys.* **158**, 341 (1993).
- ³³ S. R. White, *Phys. Rev. B* **48**, 10345 (1993).
- ³⁴ U. Schollwöck, *Rev. Mod. Phys.* **77**, 259 (2005).
- ³⁵ R. M. Noack and S. Manmana, *AIP Conf. Proc.* **789**, 93 (2005).
- ³⁶ K. Hallberg, *Adv. Phys.* **55**, 477 (2006).
- ³⁷ S. Szalay, M. Pfeffer, V. Murg, G. Barcza, F. Verstraete, R. Schneider, and Ö. Legeza, *Int. J. Quant. Chem.* **115**, 1342 (2015).
- ³⁸ M. Ezawa, *Phys. Rev. B* **76**, 245415 (2007).
- ³⁹ D. C. Tsui, H. L. Stormer, and A. C. Gossard, *Phys. Rev. Lett.* **48**, 1559 (1982).
- ⁴⁰ M. M. Wolf, F. Verstraete, M. B. Hastings, and J. I. Cirac, *Phys. Rev. Lett.* **100**, 070502 (2008).
- ⁴¹ S. Furukawa, V. Pasquier, and J. Shiraishi, *Phys. Rev. Lett.* **102**, 170602 (2009).
- ⁴² G. Barcza, R. M. Noack, J. Sólyom, and Ö. Legeza, *Phys. Rev. B* **92**, 125140 (2015).
- ⁴³ Ö. Legeza and J. Sólyom, *Phys. Rev. B* **68**, 195116 (2003).
- ⁴⁴ G. Vidal, J. I. Latorre, E. Rico, and A. Kitaev, *Phys. Rev. Lett.* **90**, 227902 (2003).
- ⁴⁵ P. Calabrese and J. Cardy, *J. Stat. Mech.* **2004**, P06002 (2004).
- ⁴⁶ Ö. Legeza and J. Sólyom, *Phys. Rev. Lett.* **96**, 116401 (2006).
- ⁴⁷ J. Rissler, R. M. Noack, and S. R. White, *Chem. Phys.* **323**, 519 (2006).
- ⁴⁸ L. Amico, R. Fazio, A. Osterloh, and V. Vedral, *Rev. Mod. Phys.* **80**, 517 (2008).

- ⁴⁹ F. F. Assaad and I. F. Herbut, Phys. Rev. X **3**, 031010 (2013).
- ⁵⁰ F. Parisen Toldin, M. Hohenadler, F. F. Assaad, and I. F. Herbut, Phys. Rev. B **91**, 165108 (2015).
- ⁵¹ Y. Otsuka, S. Yunoki, and S. Sorella, Phys. Rev. X **6**, 011029 (2016).